Journal of Atmospheric and Solar-Terrestrial Physics 147 (2016) 11–20

Contents lists available at ScienceDirect

Journal of Atmospheric and Solar-Terrestrial Physics

journal homepage: www.elsevier.com/locate/jastp

Nonlinear responses of mesospheric emission layers to wave disturbances

Alexey Belyaev

Institute of Applied Geophysics, Rostokinskya 9, 129128 Moscow, Russia

ARTICLE INFO

Article history:
Received 11 April 2016
Received in revised form
23 June 2016
Accepted 24 June 2016
Available online 29 June 2016

Keywords:
Atmospheric emission layers
Wave disturbance
Nonlinear response

ABSTRACT

Model-based investigations of the wave-induced responses of O(^{1}S), O_2(b,0-0) and OH(8-3) emissions have been performed. A series of digital experiments performed using the one-dimensional simulation model proposed by Liu and Swenson (2003) demonstrated that, in addition to the variable component, the wave disturbance of airglow emissions has a constant component. This component is the enhancement/depletion of the background emission intensity of an emission layer. To interpret its appearance, the simplest analytical model of airglow disturbance due to a gravity wave has been constructed. This model indicates that enhancement/depletion of the background emission intensity is a nonlinear airglow response to a wave disturbance. Its magnitude depends quadratically on the wave amplitude and can reach a few dozen percent relative to the value of the zenith brightness of the unperturbed OH(8-3)/O(^{1}S) emission layer.

1. Introduction

Airglow measurements are widely used to study gravity waves (GWs) in the mesopause region. The majority of these studies have focused on measuring quasi-monochromatic wave signatures in airglow images (Taylor and Edwards, 1991; Swenson et al., 1998; Walterscheid et al., 1999; Smith et al., 2000; Yamada et al., 2001) and their spatial and spectral characteristics (Hecht et al., 1994; Taylor and Garcia, 1995).

To analyze the relationship between airglow perturbations and GW characteristics, theoretical and modeling studies have been performed (Walterscheid et al., 1987; Schubert and Walterscheid, 1988; Tarasick and Shepherd, 1992a, 1992b; Hickey et al., 1993; Zhang et al., 1993a, 1993b; Makhlouf et al., 1995; Swenson and Gardner, 1998; Liu and Swenson, 2003; Hickey and Yu, 2005; Vargas et al., 2007; Snively et al., 2010). Frequently, an airglow response to a wave disturbance is characterized by the Krassovsky ratio η (Krassovsky, 1972) and the cancellation factor CF (Swenson and Gardner, 1998). Krassovsky ratio η defines the ratio of the relative airglow intensity perturbation $I_w/\langle I\rangle$ produced by GW to the relative volume emission rate weighted temperature perturbations. The mechanism of the airglow response cancellation, due to the finite thickness of an emission layer, is quantified by the cancellation factor CF, which is defined as the ratio of the amplitude of the relative airglow intensity perturbation $\hat{I}_w/\langle I\rangle$ to the gravity wave amplitude $\hat{T}$. Hereafter, $I_w = I - \langle I\rangle$, where the triangle brackets represent time/phase mean and $\hat{I}_w$ is the amplitude of the airglow intensity perturbations. In accordance with their definitions, Krassovsky ratio η and cancellation factor CF are inversely proportional to increases or decreases in the average airglow intensity $\langle I\rangle$. Note that it is tempting to replace $\langle I\rangle$ with the intensity of an unperturbed emission layer I_u during modeling studies.

The objective of this study is to show that $\langle I\rangle$ and I_u are finitely separated, and replacing $\langle I\rangle$ with I_u is not allowable when an emission layer is disturbed by a gravity wave. In other words, we demonstrate that the background intensity of an emission layer in the presence of a disturbing wave differs from that of an unperturbed layer. This effect of the waves on $\langle I\rangle$ is reversible, such that once the wave motion ceases, $\langle I\rangle$ reverts back to its original value of I_u. Note that previous numerical studies using a 2-D Chemistry-Dynamics model (Hickey et al., 2000; Hickey and Walterscheid, 2001) showed that a transient, dissipating gravity wave packet can induce a significant secular increase in background airglow intensity, that can be considered a nonlinear response of an emission layer to gravity wave disturbance (Huang et al., 2003). Particularly, it was demonstrated that the gravity wave-driven downward transport of atomic oxygen is the ultimate driver for the increases in the secular airglow intensity variations.

The present study was conducted using a one-dimensional simulation model-based on the approach proposed by Liu and Swenson (2003). The model simulations were made for three

E-mail address: anb52@mail.ru

http://dx.doi.org/10.1016/j.jastp.2016.06.011
1364-6826/

commonly observed (from ground and space) atmospheric emissions: O(^{1}S) (green line, 557.7 nm), O_2(b,0-0) (atmospheric band, 762 nm) and OH(8-3) (Meinel band, 737 nm). The main assumptions and computational algorithm used to simulate the wave disturbances and emission layer responses are included in Section 2. In Section 3, we present the simulation results, which are interpreted in Section 4 using the simplest mathematical model.

2. Simulation model

The major assumptions are as follows: (i) the background atmosphere is windless and (ii) the vertical distributions of the unperturbed temperature and O-, N_2- and O_2-number densities are specified by the MSIS-E-90 atmospheric model at 35 °N for spring equinox conditions (see Fig. 1).

2.1. Volume emission rate

Our modeling used the OH(8-3) and O_2(b,0-0) volume emission rates proposed by Liu and Swenson (2003). The O(^{1}S) emission rate was based on Vargas et al. (2007) and McDade et al. (1986). The basic sets of chemical reactions for each considered here emissions are presented in Appendix A.

In accordance with McDade et al. (1986) and Murtagh et al. (1990), the O 557.7 nm line volume emission rate (VER) ε_{O1} under a steady-state approximation is expressed as follows:

$$\varepsilon_{O_1} = \frac{A_5 k_1 [O]^3([N_2] + [O_2])}{(A_6 + k_5[O_2])(C'^{O_2}[O_2] + C'^{O}[O])}, \quad (1)$$

where $[N_2]$, $[O_2]$ and $[O]$ are the number densities of N_2, O_2 and O, respectively, $A_5 = 1.18\ s^{-1}$ is the 557.7 nm line transmission probability, $k_1 = 4.7 \cdot 10^{-33}\ (300/T)^2\ cm^6\ s^{-1}$ is the rate coefficient for three-body O recombination, $A_6 = 1.35\ s^{-1}$ is the inverse radiative lifetime of the ^{1}S state and $k_5 = 4.0 \cdot 10^{-12} \exp(-865/T)\ cm^3\ s^{-1}$ is the rate coefficient for ^{1}S state quenching by O_2. The $C'^{O_2} = 15$ and $C'^{O} = 221$ coefficients are empirical parameters that were determined during the ETON campaign by comparing the measured O density and 557.7 nm line volume emission rate profiles (McDade et al., 1986).

In accordance with Murtagh et al. (1990), McDade et al. (1986) and Zhang et al. (1993b), the O_2(b,0-0) VER ε_{O_2} under a steady-state approximation is expressed as follows:

$$\varepsilon_{O_2} = \frac{k_1 A_1 [O]^2 [O_2]([O_2] + [N_2])}{(A_2 + k_2^{O_2}[O_2] + k_2^{N_2}[N_2])(C^{O_2}[O_2] + C^{O}[O])} \quad (2)$$

where $A_1 = 0.079\ s^{-1}$ is the (0,0) band transition probability, $A_2 = 0.083\ s^{-1}$ is the inverse radiative lifetime of the $O_2(b^1\Sigma_g^+, v' = 0)$ state, $k_1 = 4.7 \cdot 10^{-33}\ (300/T)^2\ cm^6\ s^{-1}$ is the rate coefficient for three-body O recombination and $k_2^{O_2} = 4.0 \cdot 10^{-17}\ cm^3\ s^{-1}$ and $k_2^{N_2} = 2.2 \cdot 10^{-15}\ cm^3\ s^{-1}$ are the rate coefficients for $O_2(b^1\Sigma_g^+)$ quenching by O_2 and N_2, respectively. The $C^{O_2} = 7.5$ and $C^{O} = 33$ coefficients are empirical parameters that were evaluated during the ETON campaign (McDade et al., 1986).

The OH emission rate is calculated using McDade et al. model (1987) which was later adapted by Liu and Swenson (2003):

$$\varepsilon_{OH} = \frac{f_8 [O][O_2](k_6^{O_2}[O_2] + k_6^{N_2}[N_2])}{260 + 2 \times 10^{-11}[O_2]}, \quad (3)$$

where $f_8 = 0.29$ is the fraction of the $H + O_3$ production at the vibrational level, $v = 8$; $k_6^{O_2} = 5.96 \cdot 10^{-34}(300/T)^{2.37}\ cm^3\ s^{-1}$ and $k_6^{N_2} = 5.7 \cdot 10^{-34}(300/T)^{2.62}\ cm^3\ s^{-1}$ are the termolecular rate coefficients for ozone formation with N_2 and O_2 as third bodies.

The VER profiles of O(^{1}S), O_2(b,0-0) and OH(8-3) emissions calculated according to Eqs. (1)–(3) are presented in Fig. 2.

2.2. Wave perturbations

The canonical gravity wave vertical wave number spectrum of horizontal wind fluctuations in the mesopause region (Gardner, 1996) is shown in Fig. 3. The vertical wave number m_* partitions the spectrum into a small wave number region $m < m_*$ where its shape and amplitude are dominated by source characteristics and a high wave number region $m > m_*$ dominated by saturation effects. The typical value of m_* in the mesopause region is $m_* \approx 1/3$ rad/km (Fritts and Alexander, 2003), i.e., gravity waves with $\lambda_z \leq 20$ km can be considered saturated waves.

The static stability of the atmospheric layer is characterized by the buoyancy frequency N defined as $N^2 = -g(\Gamma - \Gamma_d)/T$. Here $\Gamma = -dT/dz$ is the actual lapse rate and $\Gamma_d = -dT/dz|_{\Theta=const} = g/c_p = 10K/km$ is the dry adiabatic lapse rate.

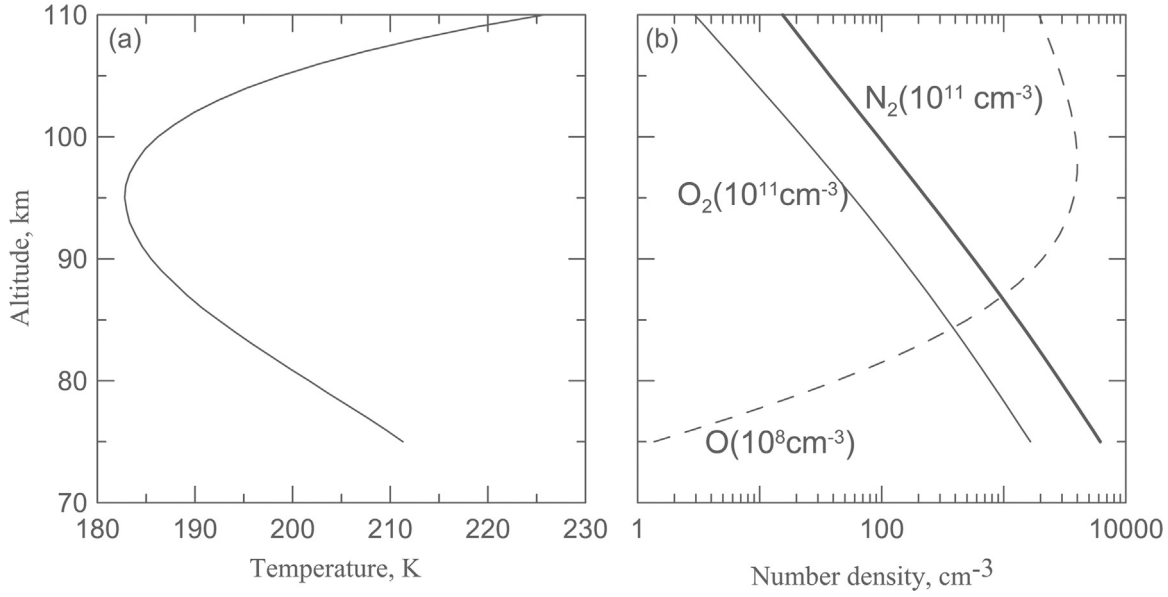

Fig. 1. (a) Temperature and (b) number density profiles of O, O_2 and N_2 based on MSIS-E-90. They are used as unperturbed states in the model.